J. Mech. Phys. Solids 187 (2024) 105623



Contents lists available at ScienceDirect

Journal of the Mechanics and Physics of Solids

journal homepage: www.elsevier.com/locate/jmps





Mechanistic understanding of microstructural effects on the thermal fatigue resistance of solder joints

Yilun Xu [a,b,*], Jingwei Xian [a,c,*], Richard J. Coyle [d], Christopher M. Gourlay [a], Fionn P.E. Dunne [a]

[a] Department of Materials, Imperial College, London, SW7 2AZ, UK
[b] Institute of High Performance Computing (IHPC), Agency for Science, Technology and Research (A*STAR), 1 Fusionopolis Way, #16-16 Connexis, Singapore, 138632, Republic of Singapore
[c] Key Laboratory of Solidification Control and Digital Preparation Technology (Liaoning Province), School of Materials Science and Engineering, Dalian University of Technology, Dalian, 116024, China
[d] Nokia Bell Labs, Murray Hill, New Jersey, USA

ARTICLE INFO

Keywords:
Crystal plasticity
Solder Joints
Thermal Fatigue
Microstructure
Multi-scale modelling

ABSTRACT

This paper uses a multi-scale crystal plasticity modelling approach to investigate the role of microstructure in the damage of Sn-3Ag-0.5Cu (wt%, SAC305) solder joints subject to thermal cycling. Faithful microstructure modelling has been developed to explicitly represent the complex microstructure characterized in the experiments. The mechanisms for the experimental finding that single crystal joints systematically outperform interlaced and beachball joints, in terms of damage development during thermal cycling, are found to be the localization of stored energy due to the grain boundaries. Interlaced regions, however, benefit the lifetime of solder joints versus a beachball microstructure by virtue of energy diffusion. The modelling results, together with experimental characterization, provide practical suggestions on how the microstructure could be designed to optimize the in-service lifetime of solder joints subject to thermal fatigue.

1. Introduction

This paper presents an integrated experimental and numerical methodology, the latter using a multi-scale crystal plasticity finite element (CPFE) approach, to investigate microstructure effects in SAC305 solder joints. Microstructure-sensitive deformation and damage are investigated for multi-grain microstructures subject to thermal cycling. The CPFE model reproduces the three-dimensional microstructures that are characterized from experimental samples using electron backscatter diffraction (EBSD) techniques. The mechanism for the detrimental effect of multi-grain microstructures on solder fatigue life is found to be the localization of stored energy at key grain boundaries. Systematic studies of interlaced microstructures (with twinned Sn orientations) and their interfaces with the package have been performed, and suggestions presented for the optimization of solder joint microstructures under thermal cycling for improved performance.

Thermal fatigue has been observed extensively in Pb-free solder joints subject to in-service loading conditions (Coyle et al., 2015; Matin et al., 2005), and limits the reliability of electronic packages and devices (Yao et al., 2017). The damage developed within solders arises from localized plastic straining which accumulates over thermal cycles (Clech et al., 2019; Gu et al., 2020), which has

* Corresponding authors.
E-mail addresses: yilun.xu@imperial.ac.uk, xu_yilun@ihpc.a-star.edu.sg (Y. Xu), jwxian@dlut.edu.cn (J. Xian).

https://doi.org/10.1016/j.jmps.2024.105623
Received 8 November 2023; Received in revised form 17 January 2024; Accepted 22 March 2024
Available online 27 March 2024
0022-5096/© 2024 The Author(s). Published by Elsevier Ltd. This is an open access article under the CC BY license (http://creativecommons.org/licenses/by/4.0/).

been shown to result from the mismatch of the coefficient of thermal expansion (CTE) between solder joints, the PCB and the package (Coyle et al., 2015) and the strong anisotropy of the elastic and plastic properties of β-Sn grains (Bieler et al., 2012). In joints under similar loading conditions (that is, with similar distances to the neutral point) containing only one (i.e. single crystal) or three (i.e. beachball) SAC305 grains, the thermal damage within individual solder joints is strongly microstructure-sensitive (Bieler et al., 2008), and is governed by crystallographic orientation combinations (relative to each other and the loading conditions), and intermetallic (IMC) size and morphology. The performance of single crystal solders under thermal fatigue has been shown to be strongly dependent on their c-axis (i.e. [001] direction) orientation with respect to the PCB (Bieler et al., 2008) and to the neutral point (Xu et al., 2022c). As a consequence, harnessing of β-Sn orientations through solidification control (Ma et al., 2017) has been proposed for improving the thermal resistance of single crystal solder joints. Recent experimental work on a ball grid array (BGA) package with SAC305 joints (Xian et al., 2023) has demonstrably shown that multi-grain joints develop more intensive damage compared to those which are single

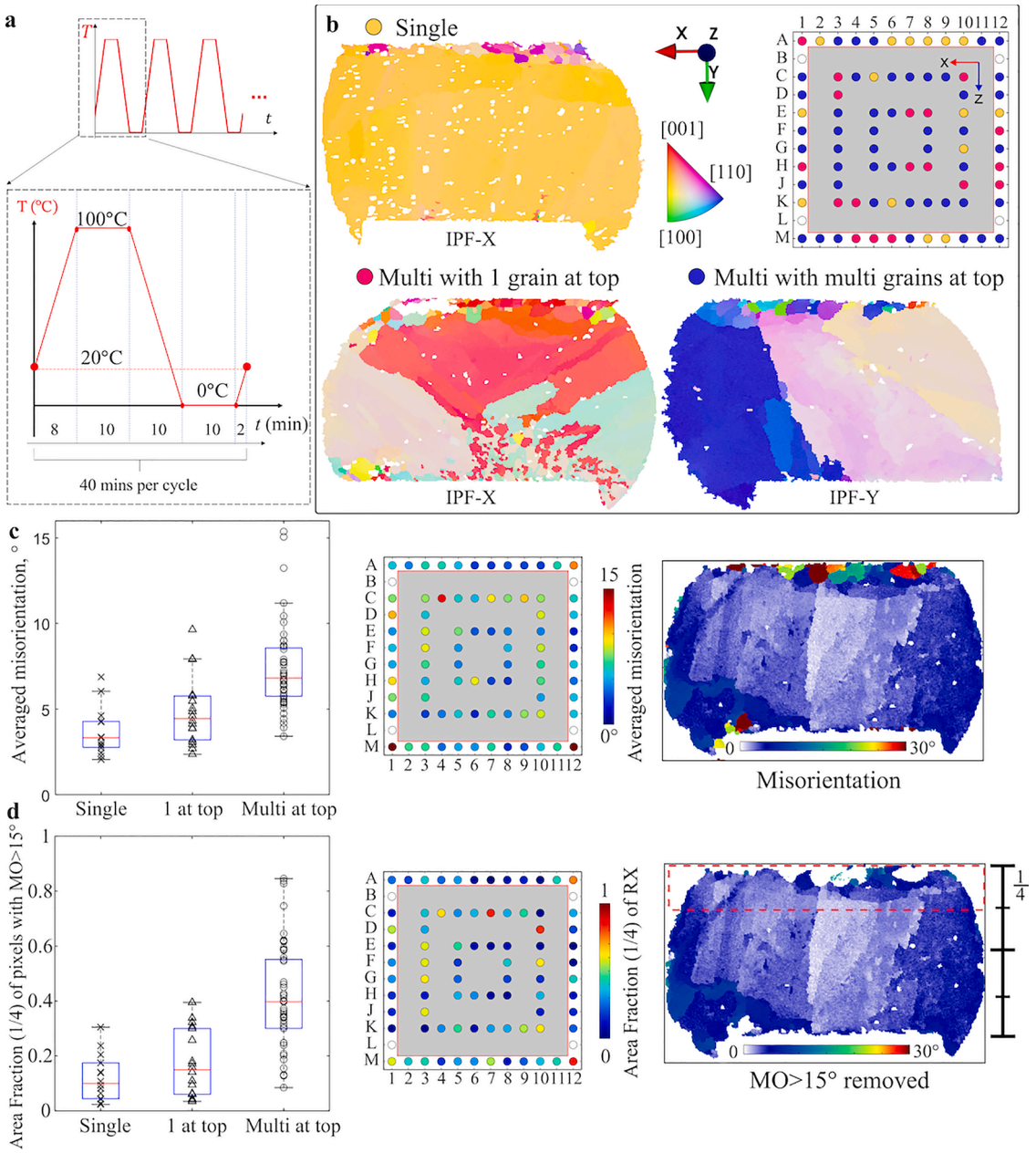


Fig. 1. (a) Thermal cycles applied to the 84CTBGA. (b) EBSD orientation maps with inverse pole figure colouring of three typical solder microstructure types after thermal cycling in the 84CTBGA. The damage, in terms of averaged misorientation (MO) in each joint (c) and the area fraction of recrystallisation in the top quarter of each joint (d) in different microstructure types of solder joints. In (b)-(d), the pin diagram is coloured by the relevant quantity at each joint position in the array.

crystal under thermal cycling. However, the factors controlling degradation of multi-grain solder joints have yet to be fully identified due to the complexity and uniqueness of microstructure at each position in the array, and the role of interlaced regions on the thermal fatigue life of solder joints has not yet been addressed.

Crystal plasticity finite element (CPFE) modelling has been widely used to investigate the anisotropic micro-scale deformation and damage of solder material and joints made up of SAC305 under thermomechanical loading. Xie et al. (Xie and Chen, 2022; Xie et al., 2022) proposed a temperature-dependent, homogenized and dual-phase crystal plasticity model, which captures the thermal aging and asymmetry of tension-compression effects in solder joints subject to thermal fatigue. Multi-scale CP models (Jiang et al., 2022; Xu et al., 2022c) were developed to investigate single crystal solder joint behaviour and highlighted the role of crystallographic orientation on the damage development over thermal cycles. Numerical approaches (Darbandi et al., 2013, 2014) have been utilised to represent the microstructure of multi-grain solder joints (Lehman et al., 2010) but model the microstructure from two-dimensional EBSD maps only. Hence fully three-dimensional microstructural representations of multi-grain solders have yet to be developed in order to investigate the role of the microstructure, and notably morphology, in solder damage. A microstructure-sensitive driver for fatigue crack nucleation, namely stored energy density (Xu et al., 2021c), has been utilised to quantify the damage developed within single crystal solder joints subject to thermal cycling, and the arising geometrically necessary dislocation (GND) density has been associated with resulting localized recrystallization (Xu et al., 2022c). However, fatigue in solder joints with more complex microstructures, and in particular those with interlaced features, has yet to be mechanistically understood, and interlaced fatigue lifetimes in relation to single crystal, or beachball solder microstructures remains to be explained and predicted.

In the following, a brief summary of the experimental set-up and key results of characterization are given in Section 2. The modelling methodology is described in Section 2.2, which highlights the approach for fully three-dimensional microstructural model representation of multi-grain solder joints, with microstructures matching the experimental characterization. Section 4 investigates the roles of grain boundaries, interlaced regions and interfaces on microstructure-sensitive damage development in solder joints subject to thermal cycles. This is followed by remarks and suggestions for optimizing solder joint microstructures in the conclusions.

2. Experiments

2.1. Thermal cycling test vehicle and characterization

The ball grid array component (84CTBGA) is a thin core package with planar dimensions 7 × 7 mm, supporting 84 solder joints of size ~360 μm and pitch 500 μm as shown in Fig. 1(a). The technical details of the test vehicle that include the board, package, attachment process and reflow parameters can be found in (Coyle et al., 2016). The BGA board was thermally loaded with the temperature cycle schematically shown in Fig. 1(a), which is representative of in-service conditions for telecoms applications. The BGA board was thermally cycled within extremes of 0°C and 100°C, with 10-minute dwell time at both extreme temperatures. The heating and cooling rates were controlled to be 10°C / minute, and such low rate normally gives a uniform temperature distribution within the PCB, package and solder joints (Sidhu and Chawla, 2008). Therefore, the temperature gradient within solder joints, or thermal shock, is not considered in the numerical modelling.

After 7580 thermal cycles, the BGA component was mounted vertically in resin and incrementally ground to the centre of each row of joints starting with row M (see Fig. 1(b)). The cross sections were investigated with a Zeiss Sigma300 field emission gun scanning electron microscope (FEG-SEM). Crystallographic orientation information was studied using a Bruker e-Flash electron backscatter diffraction (EBSD) detector and analyzed using Bruker EPSRIT 2.1 software and the MTEX toolbox in MATLAB.

Typical EBSD orientation maps of solder joints can be found in Fig. 1(b), using inverse pole figure (IPF) coloring. Note that the labels “single grain” and “multigrain with a single orientation at the top” refer to the original soldered microstructures and that the small grains at the top of the joints (the package side) formed due to recovery and recrystallisation during thermal cycling. The major β-Sn orientations in each joint to be modelled were measured from the EBSD maps and are summarized in Table 1, where β-Sn tri-orientations (e.g. K3 and M7) constitute a single-ring beachball microstructure and the five β-Sn orientations (e.g. C7) generate a mutual-twin double-ring beachball microstructure. Note that the coordinate system in Fig. 1(b) was rotated by 180° with respect to the z-axis to unify the EBSD measurements and later Abaqus modelling. To evaluate the microstructural effects and explore the underlying mechanisms, 3D geometrical models for these multi-grain joints were constructed based on EBSD measurements on 2D sections and

Table 1
Summary of the type and crystallographic orientations (with reference to the coordinate system shown Fig. 1b) of the investigated solders on the BGA ball array subject to thermal cycles. K3 and M7 are single-ring cyclic twins. C7 involves a double ring of cyclic twins.

Solder	Type	Crystallographic orientations (by Euler angles)				
A6	Single crystal	72,40,156				
A7		17,66,220				
A8		292,76,308				
A9		245,46,44				
M8		67,57,49				
M9		103,56,30				
K3	Cyclic twinned	139,56,163	188,83,54		63,62,208	
M7		356,48,78	61,75,43		281,63,129	
C7		203, 32, 95	271,63,42	130,72,138	26,21,266	24,80,266

knowledge of the 3D crystallographic geometry of beachballs using the method introduced in (Xian et al., 2023). Crystal plasticity finite element models were subsequently established to reproduce the three-dimensional geometrical models.

2.2. Key experimental findings

The experimental findings from this 84CTBGA from (Xian et al., 2023) are visualised in Fig. 1(b)-(d) by colouring joint positions in the pin diagram by their measured features: their microstructure type (1(b)), the mean misorientation (MO) with respect to the main orientation(s) in the joint (1(c)), and the area fraction of recrystallisation defined as the area fraction with MO $> 15°$(1(d)). Note that the developed MO and recrystallisation are markedly different in joints in symmetrically equivalent positions (e.g. compare joints C4, C9, K4, K9) showing that damage depends significantly on microstructure as well as on the location in the array. From the box plots with overlaid datapoints, we see that, in general, single grain joints developed the least damage, multi-grain joints with a single orientation at the top accumulated more damage, and multi-grain joints with multiple orientations at the top accumulated the most thermal fatigue damage. We also see overlap in the data between joints in these three categories which is due to additional factors such as the crystallographic orientation of the grain(s) that are not shown in Fig. 1(c-d). We next explore the mechanistic basis for these results with the CPFE model by first examining individual solder joints in detail and then performing a parameter study whereby the boundary conditions are kept constant, and the microstructure is systematically changed. The latter applied the boundary conditions to single crystal, beachball and interlaced variants as well as up-side-down variants.

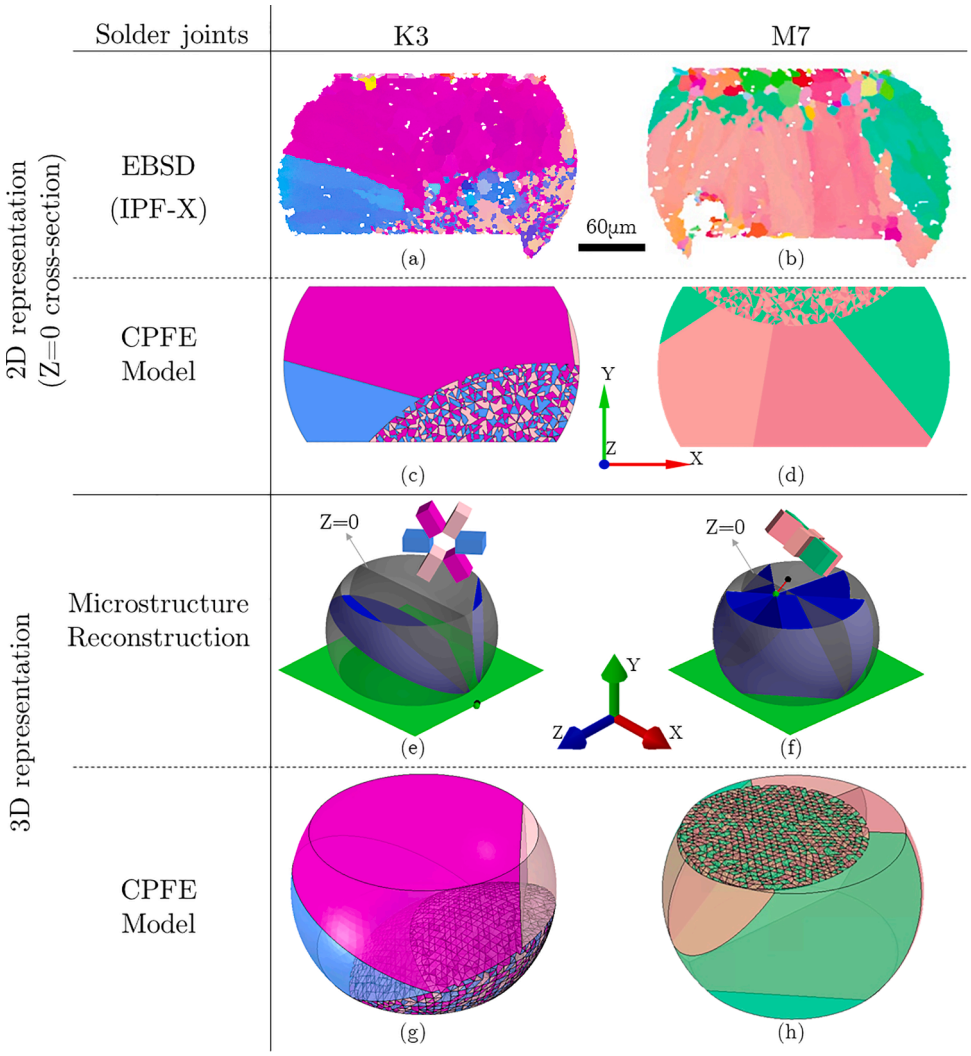


Fig. 2. Microstructure characterization and modelling of multi-grain solders K3 and M7. The EBSD maps (IPF-X) are shown in (a)-(b) and the corresponding cross-section views ($Z = 0$ as the cut plane) of the CPFE models are shown in (c)-(d). The reconstructed three-dimensional microstructures with measured β-Sn wireframes (Xian et al., 2023) are shown in (e)-(f) and the corresponding microstructure models are shown in (g)-(h). The black lines in the model outline the grain boundaries i.e. among SAC305 grains with different crystallographic orientations.

3. The crystal plasticity modelling method

3.1. Multi-scale modelling strategy

A multi-scale modelling approach has been used to transfer the temperature fields applied on the BGA board to the displacements at both top and bottom interfaces of individual solders (Xu et al., 2022c). More than 100 thermal cycles have been modelled at the BGA board-scale model, and the transferred displacement fields found to stabilize after five cycles. Therefore, the stabilized displacement fields are imposed on the individual solders according to their specific locations (see Fig. 1(b)) as cyclic boundary conditions for the following consecutive five cycles (i.e. 6th – 10th cycle). Due to the complexity and variety of the multi-grain solder microstructures (see Fig. 1(b)), the displacement boundary conditions are passed by virtue of using a three-degree bivariate (as the coordinates of X and Y) polynomial fitting as opposed to a node-wise style (i.e. the accurate mapping) along the top and bottom faces. The accuracy of the polynomial approximation (i.e. the fitting of the displacement fields against the node-wise mapping) has been justified by comparing the displacement component fields that are imposed to the model and the resulting plastic strains that are obtained from the model. The details of the fitting and comparison can be found in Fig. A 1.

All the solder joints investigated are assumed to have the same geometry and dimensions, and the joint shape and representative dimensions are assigned to them, shown in the last row of Fig. 2. Each individual solder joint is discretised using 2nd order, tetragonal-shaped finite elements (named as C3D10 in the ABAQUS library) with the element size (i.e. the edge length of the tetrahedron) of ≈ 4 μm. A non-local methodology (Xu, 2021) is used to overcome the calculation difficulties in finding geometrical necessary dislocation (GND) density within tetrahedron-shaped finite elements, which minimizes the mesh size dependency. The establishment of the microstructure of interlaced solder joints and the crystal plasticity formulations that describe the microstructure-dependent behaviours are detailed in Section 3.2 and 3.3.

3.2. Microstructure modelling for interlaced solders

The microstructural models were reconstructed using the method described in detail in (Xian et al., 2023) which combines the two-dimensional cross-section information of orientations and {101} grain boundary traces measured from an EBSD map (Fig. 2 (a)-(b)) with the three-dimensional information of the crystallographic geometry of cyclic twinned β-Sn determined in past work (Lehman et al., 2010). The reported beachball microstructure served as the prototype of the 3D model and the underlying idea of the reconstruction method is equivalent to digitally rotating and translating the beachball microstructure (Lehman et al., 2010) to generate a digital cross section satisfying the measured Sn orientations and 2D grain boundaries using EBSD. More details in confirming {101} Sn grain boundaries as the beachball boundaries can be found in (Xian et al., 2023). Note that at least two near-linear 2D grain boundaries (e.g. Fig. 2e-f) are needed in the EBSD map to geometrically identify the nucleation position and the unique orientation of the 3D trial-crystal beachball. The latter is approximated as three orientations related by 120° rotations around a common <010> axis with {101} grain boundaries (Fig. 2(e)-(f)). This leads to three to six 3D segments in total for a 'single ring' beachball with the common <010> axis and all {101} boundaries intersecting at a point on a Cu_6Sn_5 layer, where the β-Sn nucleates (Xian et al., 2017). This is shown for joints K3 and M7 in Fig. 2 where the nucleation point is on the bottom Cu_6Sn_5 layer for K3 and the top layer for M7 as marked by the green dots in ((c)-(f)). For 'double ring' cyclic twinned microstructures such as C7 in Table 1, a similar procedure was followed but using the two common <010> axes measured by EBSD.

Interlaced regions are realized by an intersection between the established beachball and a sphere of interlacing with an appropriate radius and centre position such that the 2D cross sections in the CPFE model ((c)-(d)) visually resemble those characterized in the corresponding EBSD maps. Tetrahedron-shaped elements are used to discretize the interlaced region, and a set of neighbouring elements is defined as interlaced grains with a representative experimentally quantified size. A random distribution of mutually twinned crystallographic orientations is assigned to the grains within the interlaced region, which reflects the EBSD measurements. The 3D representations of the partially-interlaced solder joints are shown in (g) – (h) for K3 and M7, respectively, and the details for modelling a multi-grain solder joint are given in Fig. A 2 with joint K3 taken as an example.

3.3. Crystal plasticity formulations

A crystal plasticity framework that is both dependent on strain-rate and temperature is used in the present study for modelling the SAC305 grain behaviour (i.e. β-Sn plus embedded Ag_3Sn and Cu_6Sn_5 intermetallics) within individual solder joints. The slip rate sensitivity is based on the thermal activation of dislocation escape from obstacles (Dunne et al., 2007), and the details can be found in previous research (Xu et al., 2022c). As a consequence, only the key aspects are given below.

The plastic velocity gradient tensor $\boldsymbol{L^P}$ at any instant takes the sum of projected slip rates $\dot{\gamma}^{(i)}$ along all slip systems within SAC305 grains, which gives:

$$\boldsymbol{L}^p = \sum_{i=1}^{M} \dot{\boldsymbol{\gamma}}^{(i)} \boldsymbol{s}^{(i)} \otimes \boldsymbol{n}^{(i)} \tag{1}$$

where M is the total number of potential slip systems (up to 32 for the β-Sn (Zhou et al., 2009) phase in SAC305 grains), and $\boldsymbol{s}^{(i)}$ and $\boldsymbol{n}^{(i)}$ the shear and normal unit vectors of the i^{th} slip system, respectively. The slip rate $\dot{\gamma}^{(i)}$ along the i^{th} slip system is determined by thermal

activation (hence temperature-dependent) events of dislocation jumping over obstacles both forward and backward, and its value is calculated as:

$$\dot{\gamma}^{(i)} = \rho b^2 v_D \exp\left(-\frac{\Delta H}{k\theta}\right) sinh\left(\frac{\Delta V}{k\theta}\left|\tau^{(i)} - \tau_c^{(i)}\right|\right) sign\left(\tau^{(i)} - \tau_c^{(i)}\right) \tag{2}$$

where ρ is the mobile dislocation density, b the magnitude of the Burgers vector of the ith slip system (i.e. varying with slip systems), ν_D the dislocation attacking frequency, ΔH the activation energy, ΔV activation volume, k the Boltzmann constant, θ the temperature and $\tau^{(i)}$ is the resolved shear stress (and critical resolved shear stress with subscript c) calculated as the Cauchy stress tensor projected onto the i^{th} slip system. The critical resolved shear stress $\tau_c^{(i)}$ evolves with total dislocation density (including the contribution of both statistically stored dislocations (SSD) and geometrically necessary dislocations (GND)) through a Taylor hardening law, where SSDs evolve with plastic strain while the GNDs carry the lattice curvature and reflect the local plastic strain gradient during plastic deformation.

Two main microstructure-sensitive measures, namely the mis-orientation (MO) and stored energy density (SED), are employed in the present study to quantify the fatigue damage of solder joints subject to thermal cycling. The mis-orientation is directly associated with the GND density (Kysar et al., 2007), and has been shown to be strongly correlated to fatigue crack nucleation in single crystal solder joints (Xu et al., 2022c). The stored energy density provides a mechanical measure, which integrates the contribution of dislocation slip and interaction within a dislocation structure where energy is stored (Xu et al., 2021c), to quantify the required energy for crack-related surface (i.e. Griffith-like criterion) generation. It has been utilized to reveal the mechanisms for fatigue crack nucleation (Prastiti et al., 2020; Xu et al., 2024) and short crack growth in various alloys e.g. (Wilson and Dunne, 2019). The energy density G is given by:

$$G = \int \frac{\xi\boldsymbol{\sigma} : d\boldsymbol{\varepsilon}^p}{\sqrt{\rho_{ssd} + \rho_{gnd}}} \tag{3}$$

where ξ is the fraction of plastic work stored in a dislocation structure and estimated as 0.05 (Kamlah and Haupt, 1997), ρ_{ssd} and ρ_{gnd} the density of statistically stored dislocation and geometrically necessary dislocation, respectively. The stored energy density has been shown to be a faithful microstructure-sensitive quantity to predict the potential crack nucleation sites, which are strongly dependent on crystallographic orientation, within Sn-rich solder joints through comparison to micro-scale experiments (Xu et al., 2022c). It is noted that the critical stored energy is temperature-dependent that is associated with surface energy.

The crystal plasticity properties of SAC305 grains have been established through a multi-scale homogenization of anisotropic β-Sn phases and intermetallics (including Cu_6Sn_5 and Ag_3Sn phases), of which the former were extracted from an integrated modelling and experimental study of single crystal micro-pillars (Xu et al., 2022b) at room temperature. The temperature sensitivity (up to 120°C) of the slip strengths and moduli are taken from independent research (Xie et al., 2021). The anisotropic material properties (in terms both of elasticity and plasticity) for the homogenized SAC305 single crystal at room temperature are given in Table 2. The CPFE model (Xian et al., 2023) and the temperature-dependent material properties capture the mechanistic basis of the effects of intermetallic size and morphology as demonstrated previously on the creep response of directionally solidified SAC305 samples (Xu et al., 2021a).

4. Results and discussion

The SED distributions and path variations are shown in Fig. 3 for the three multi-grain solder joints M7, K3 and C7 at the end of the 10th cycle. The SED is highly localized near the circumference of the top interface for all three solders, which arises from the difference of CTE between Sn grains and between the solder joints and PCB and/or package (Yao et al., 2017). In addition to the circumference, the grain boundaries also contribute to localization of SED (see the red arrows in (d)-(e) as an example), which indicates the potential fatigue crack nucleation sites near top interfaces within solders (Borgesen et al., 2018). Among the three solder joints, there are noticeably high energy peaks (indicated in (g)) identified in solder joint C7 showing in the SED image along the A-A 'path. Solder joint C7 has a "double-ring" microstructure feature (Xian et al., 2023) containing five major grain orientations (see Table 1) while solders M7 and K3 have a "single-ring" cyclic twin microstructure containing three grain orientations (see Table 1). The SED localization by virtue of the grain orientation inhomogeneity within solders may provide the mechanical basis for the outperformance of the single ring compared to the double ring microstructure on the thermal fatigue resistance.

Mis-orientations (MO) that are characterized as the crystallographic orientation differences against the centre region have been associated with recrystallization within solders in our previous study (Xian et al., 2023; Xu et al., 2022c), and they can be quantitatively predicted from the local geometrically necessary dislocation density (Witzen et al., 2020) through a numerical method

Table 2
Material properties for SAC305 single crystal (β-Sn with embedded Ag_3Sn and Cu_6Sn_5) at room temperature 25°C.

(GPa)	E_{33}(GPa)	G_{12}(GPa)	G_{13}(GPa)	$\tau_{c0}^{(2,3)}$(MPa)	$\tau_{c0}^{(8,10)}$(MPa)
26	70	24	22	4.8	7.5
$\lambda_1(\mu m^{-2})$	$\lambda_2(\mu m^{-2}s^{-1})$	$\rho(\mu m^{-2})$	$k(JK^{-1})$	ΔH	ΔV
750	100	1.2	1.38×10^{-23}	41 kJ/0.42eV	$9.26b^3$

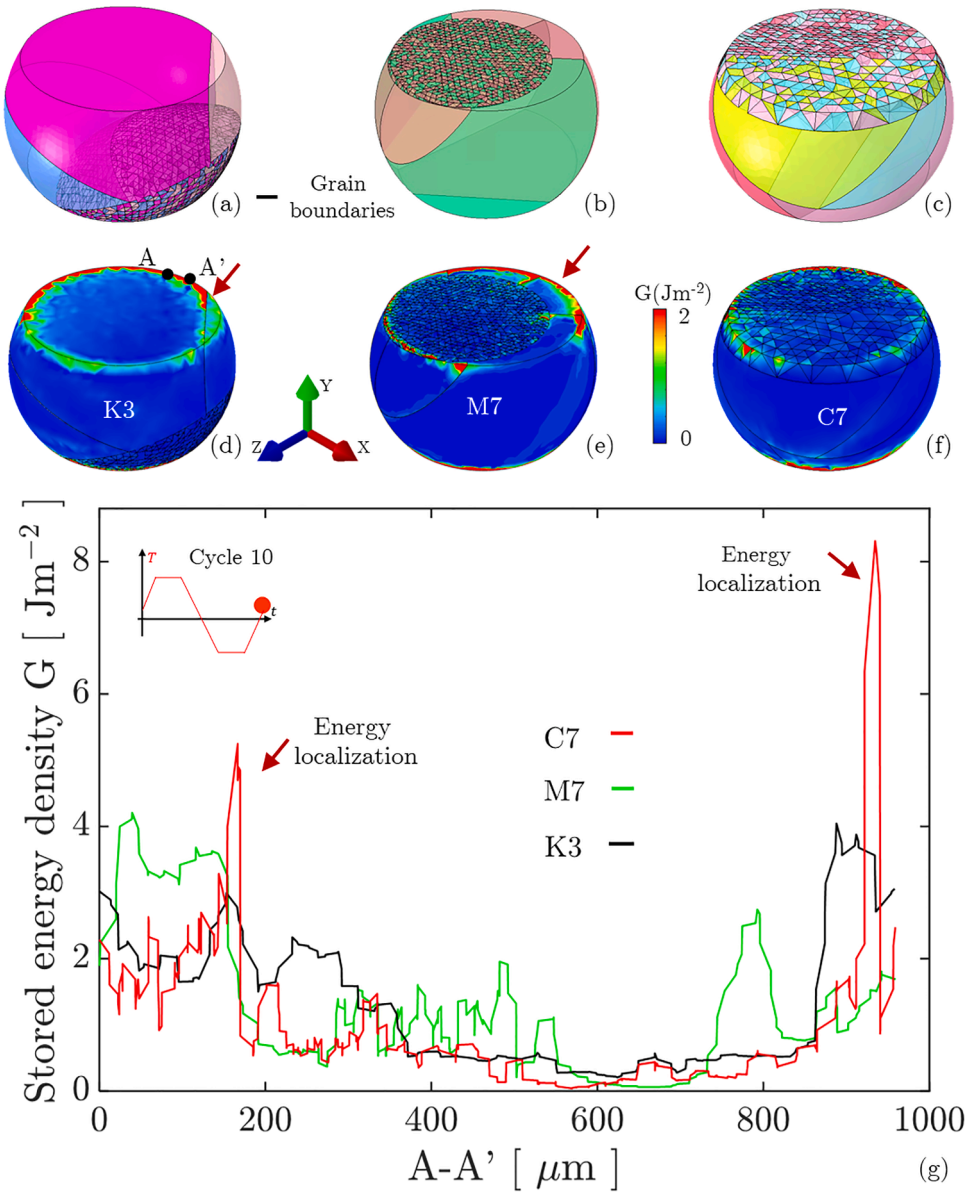


Fig. 3. The microstructure models for solder joint K3, M7 and C7 are shown in (a)-(c). The black lines in the model indicate the grain boundaries i.e. among SAC305 grains with different crystallographic orientations. The stored energy developed with the investigated solder joints (d) K3, (e) M3 and (f) C7 at the end of 10th thermal cycle, the former two having a "single-ring" grain orientation combination and the latter has a "double-ring" grain orientation. The stored energy distribution along the circumference (A-A') is shown in (g) for the three solder joints.

(Pantleon, 2008). The MO section maps of the multi-grain joints M7, K3 and C7 are shown in Fig. 4(a) – (c), respectively, after 7580 thermal cycles. The experimental findings indicate the recrystallization primarily takes place near the top interface (i.e. package-side) and secondarily at the bottom of the solder, and the interlaced region facilitates a more diffuse recrystallization process from the top into the bulk of solders (see (c) for joint C7 as an example). The corresponding MO maps that are predicted using the CPFE model are shown in Fig. 4(d) – (f) at the end of cycle 10. The distribution of the predicted mis-orientations satisfactorily resembles the characterization in the experiments, highlighting the localization of MO at both the top and bottom interfaces. In addition, the mis-orientation developed in K3 is found to be much lower than those in M7 and C7, which correctly reflects the fatigue life trend (Xian et al., 2023). The difference of mis-orientation predicted near the bottom interface in joint K3 between the CPFE and EBSD analysis might arise from the effect of pores (see the EBSD in (a) as an example) or micro-scale intermetallics that have not been characterized in the EBSD scan. The considerable concentration of MO is spotted within the interlaced region that is caused by the inhomogeneity of developed plastic strain and hence resulting plastic strain gradient during thermal cycles. Compared to those developed in single crystals (Xu et al., 2022c), the MO distribution in the multi-grain solders shows a generally higher magnitude and more influence in the

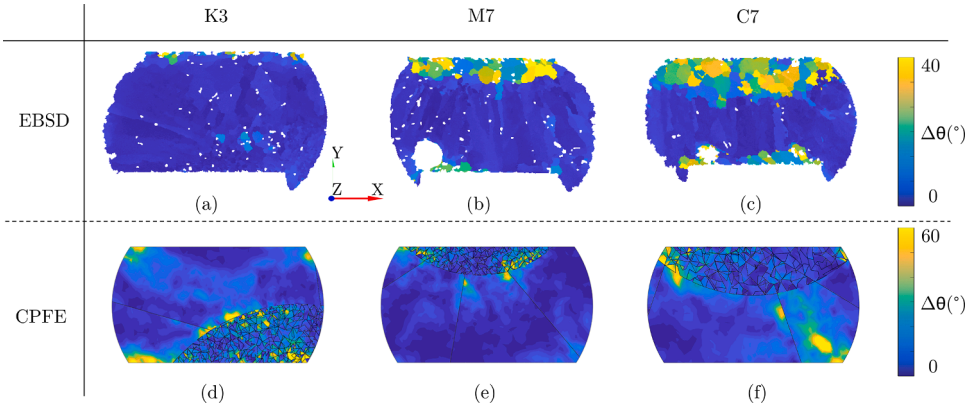


Fig. 4. The mis-orientation developed in Solder K3, M7 and C7 analysed from EBSD data (a) – (c), and predicted using the CPFE model through the analysis of geometrical necessary dislocation density (d) – (f), respectively.

bulk, hence intensively recrystallised and damaged as shown in Fig. 1(c) and (d) for solder M7 and C7. Therefore, it would be potentially beneficial to avoid the multi-grain microstructures through control of solidification.

Solder joint C7, which consists of five grain orientations that are mutually twinned in a "double-ring" orientation relationship (OR), was reconstructed in the crystal plasticity modelling into eight microstructure 'variants', Fig. 5(a): (i) the experimentally measured microstructure with a partially-interlaced region (i.e. the 2nd row in (a)); (ii) a beachball obtained by digitally removing the interlacing (i.e. the 3rd row in (a)); (iii) a fully-interlaced variant realized through assigning the whole solder joint with the five given crystallographic orientations (i.e. the 1st row in (a)), using an interlacing spacing that follows a random distribution with a mean value of 7 μm that reflects an independent characterization (Shang et al., 2017); and (iv)-(viii) single crystal variants each with one of the five grain orientations in joint C7.

The SED developed within solder joint C7 and its synthesised microstructure variants are shown in Fig. 5. The grain boundaries are found to localize the SED both along the circumference and over the top faces, which gives rise to the high SED (near the regions labelled as P, R and Q) within the partially-interlaced solder joint (real) and beachball microstructures compared to the synthesised single crystal cases. The SED within the beachball microstructure shows a highest peak near the grain boundaries intersecting the top faces, which are labelled as Q in (a). This suggests that the presence of the interlaced region would benefit the thermal fatigue life of multi-grain solder joints by diffusing the energy stored within the interlaced grains as opposed to exacerbating the energy distribution. The effect of the interlaced region on relieving energy concentration is slightly enhanced in the variant of the fully interlaced case. This finding from the simulations is in agreement with past experimental studies on accelerated thermal cycling of SAC solder joints that have reported that joints with interlaced Sn grain morphology have longer thermal fatigue life compared to beachball microstructures (Arfaei et al., 2013a, 2013b) as the interlaced region delays fatigue crack nucleation. The generally low stored energy developed within the single crystal joints in Fig. 5 again suggests the negative effect of grain boundaries on the life of the multi-grain solder joints.

The top interface between solder joints and the package has been identified as a preferred location where fatigue cracks likely nucleate during thermal cycles in both experiments (Bieler et al., 2012; Branch Kelly et al., 2020; Coyle et al., 2015) and in modelling of single crystal solder joints (Lövberg et al., 2017; Stoyanov et al., 2020; Xu et al., 2022c). To explore the role of the microstructure near the top interface, the microstructure variants of K3 were modelled as the experimentally determined partially interlaced microstructure, a beachball variant (without the interlacing) and as their up-side-down realizations, i.e. by rotating the solder joint 180 degrees with respect to the Z-axis such that the microstructure at the top interface differs but the boundary conditions remain the same. The resulting SED contours are shown in Fig. 6. The grain boundaries, in addition to the circumference of the top faces, are found to facilitate SED developing locally ((a) viewed in 3D and (b) viewed from the top). The distribution of SED along Path A-A' i.e. the circumference (indicated in (a)) is compared in Fig. 6(c) among the K3 variants including the single crystal variants. All beachball and interlaced solder joints (solid lines) develop considerably higher SED compared to models with a single crystal microstructure (dashed lines). The up-side-down variant of the beachball microstructure (labelled as green line) shows a sharp spike of SED located near the triple junction (indicated as P in (a)) of grain boundaries at the top face, and the beachball one shows a sharp peak near the grain boundary intersection (indicated as Q in (a)). The up-side-down realization of the interlaced beachball, however, despite having a large number of intersections at the top interface, is found to develop a comparable SED level with the real solder microstructure, where its top face is free of intersections. Therefore, it is of importance to optimize the microstructural morphology near the top surface of solder joints.

Significant microstructural change has been quantified near the top interface in the solder joints subject to thermal cycles (Xian et al., 2023), which is consistent with previous findings (Arfaei et al., 2013b; Chen et al., 2011; Sundelin et al., 2008; Zhou et al., 2015). The microstructure change that manifests itself as the developed misorientation has been associated with the localized geometrically necessary dislocations in single crystal solder joints (Xu et al., 2022c), but the role of shear stress, which is commonly observed in thermally damaged solder joints (Qi et al., 2009), on the misorientation development has yet to be revealed. The mis-orientation maps of solder joints M7, K3 and C7 that were characterized using EBSD are shown in Fig. 7(a)-(c) and the corresponding in-plane shear

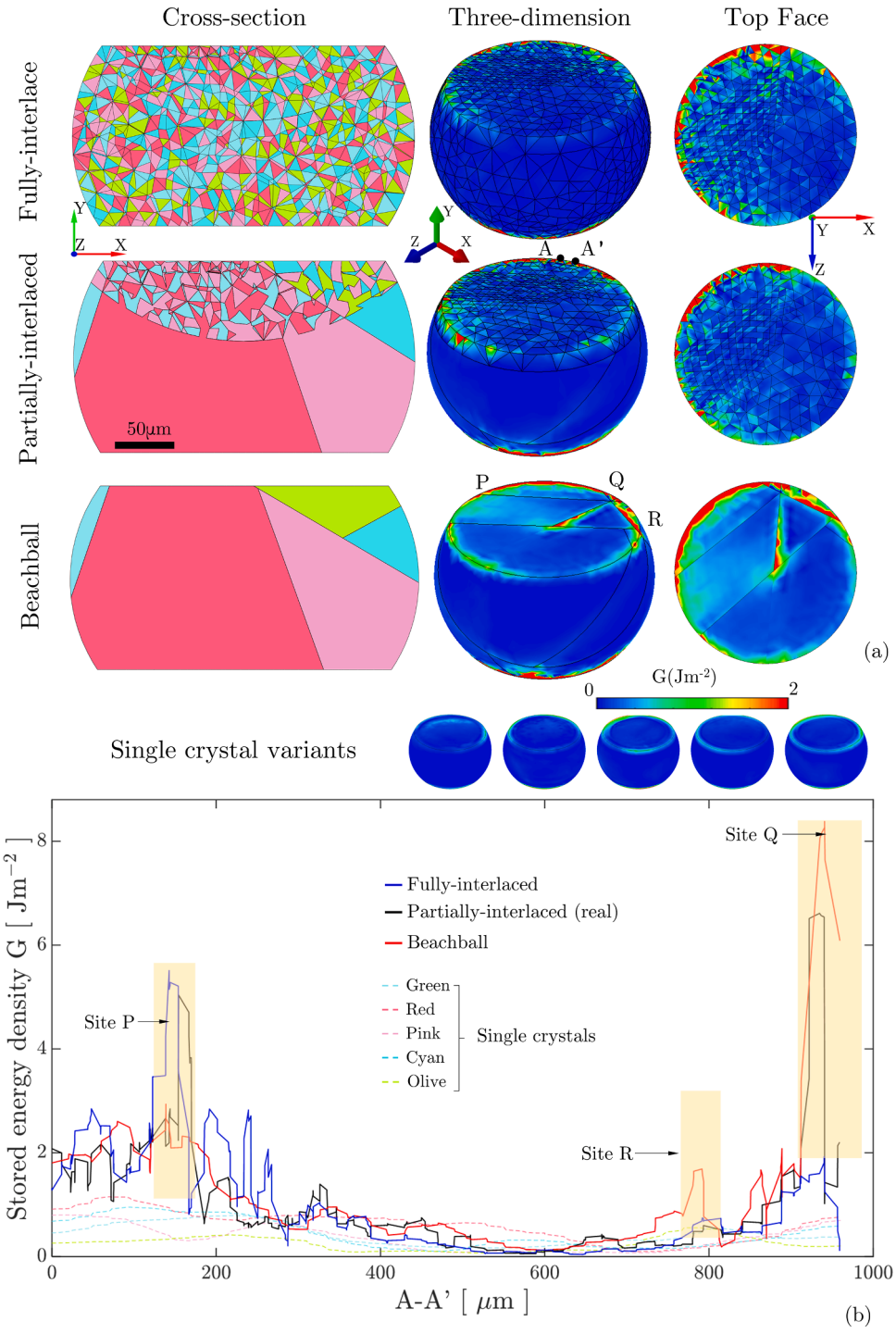


Fig. 5. The effect of the microstructural morphology on the damage of solder joints. Solder joint C7 and its synthesis variants are taken as example. The cross-section view of the microstructure, the three-dimensional view of the stored energy contours and the stored the energy distribution on the top face of solder joint C7 and its beachball variant. The stored energy contours of the single crystal variants are also included for reference. (b) the distribution of the stored energy density along the circumference of the top interface of solder joint C7 and its variants. Results are obtained at the end of 10th cycle, and the single crystal results are included for reference.

stresses along the X-Y cross-section are shown in Fig. 7(d)-(f). The recrystallization is found to be localized at the top interfaces and its sub-surface regions while limited in the bulk of the solder joints, which is aligned with the distribution of shear stresses. The grain boundaries give rise to additional shear stress concentration within the interlaced regions, which may contribute (through high stored

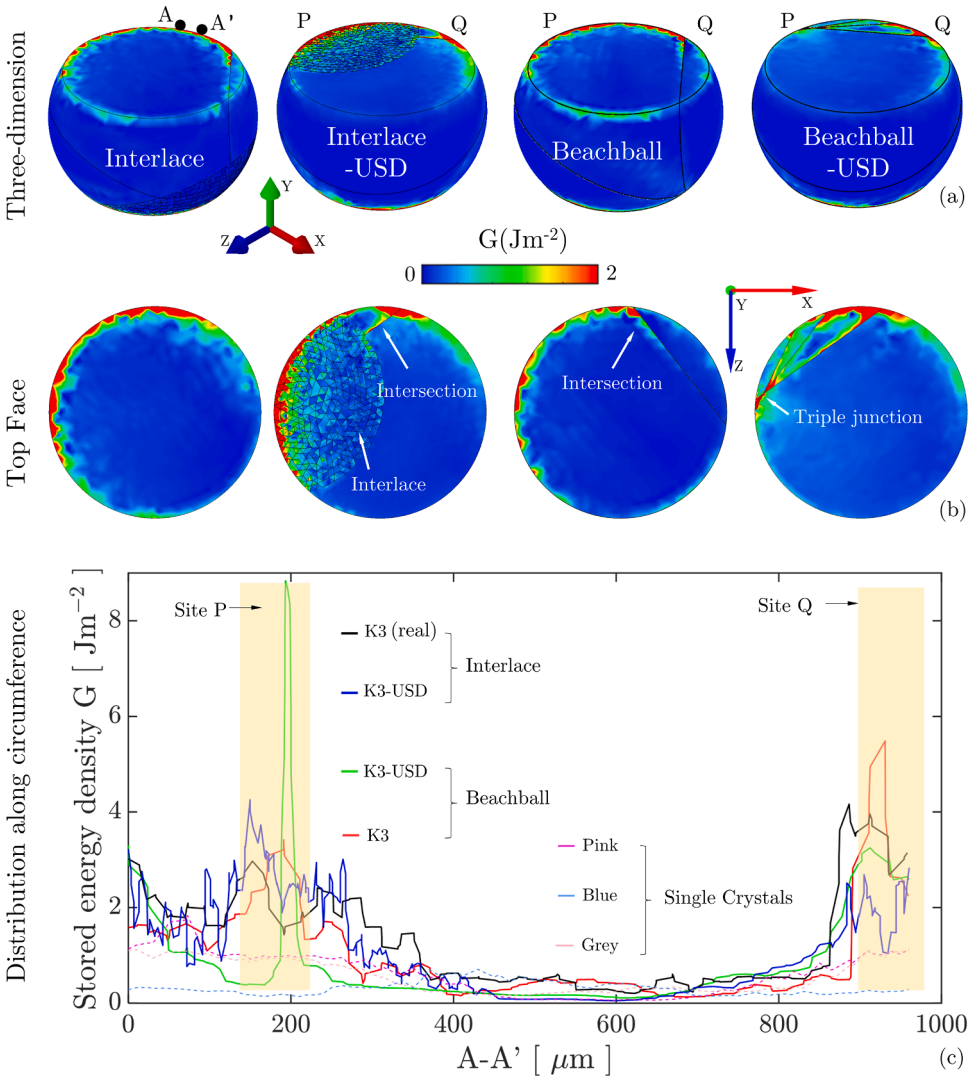


Fig. 6. The interface effect on the damage within solder joints subject to the thermal cycling. The stored energy density developed by solder joints K3 and its variants, which include the 'up-side-down' (USD) microstructure, the beachball microstructure, the 'up-side-down' beachball microstructure and single crystals, (a) within the solder joints in three-dimensional view, (b) along the top faces, and (c) the distribution of the stored energy density along the circumference of the top interface. Results are obtained at the end of 10th cycle.

energy) to the recrystallization process. Shear stresses have been shown to induce confined plasticity developed at the interfaces and sub-surfaces through dislocation pile up (Zhang et al., 2014) that were revealed by STEM experiments (Ruebeling et al., 2021) and discrete dislocation plasticity (Xu et al., 2021b), and the local plasticity results in considerable lattice rotation (up to 25°) and eventually recrystallization within alloys (Haug et al., 2022; Xia et al., 2023) when the energy is sufficient to drive it to take place (Xu et al., 2022a). The association between the recrystallization and shear stress shown above may suggest a surface-enhanced microstructure (e.g. through a gradient (Li et al., 2020) or heterogonous structure (Zhu and Wu, 2023)) would relieve the shear stress concentration and in turn benefit the lifetime of solder joints under thermal cycles.

The SED criterion has been successfully applied to explain and predict fatigue crack nucleation sites in various ductile alloys, such as ferritic steels (Wan et al., 2014), nickel-based superalloys (Jiang et al., 2016; Zhang et al., 2021) and Zircoloy (Wan et al., 2023). The sites where the SED achieves its peaks along a surface, as opposed to an average sense, would be considered to be susceptible to crack nucleation (Prastiti et al., 2020), which reflects that the SED is a microstructure-sensitive and highly localized quantity. Fig. 8 revisits the SED developed within the single crystal variants of solder joints K3, C7 and M7 subject to the corresponding thermal cycles, respectively, at the end of 10th thermal cycle. Fig. 8(a), showing the SED distribution along the top circumference of the single crystal solder joints, suggests the strong correlation between the SED developed and the crystallographic orientation. A featured SED that is quantified as the mean value of the highest 10% SEDs along the top circumference (i.e. shown in Fig. 8(a)) further highlights the leading role of the specific single crystals in Fig. 8(b). The single crystal variants of M7 systematically develops more damage compared

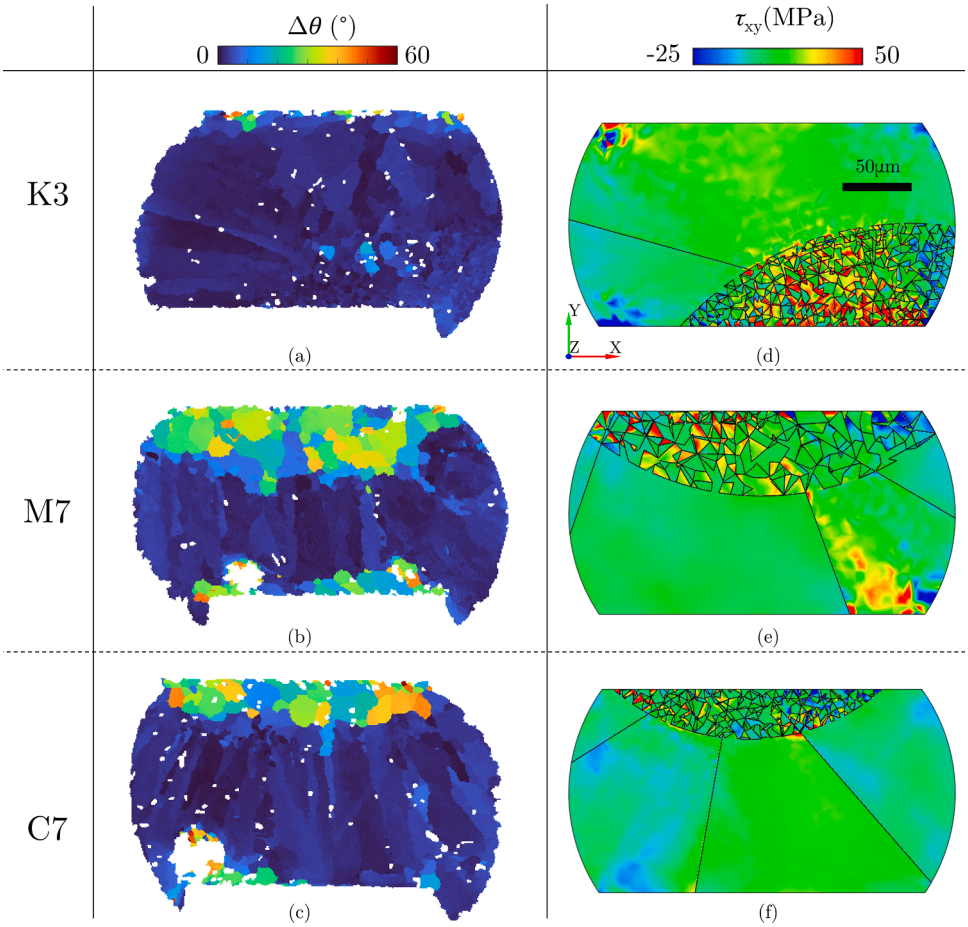


Fig. 7. The correlation between the microstructure changes through recrystallization and the local shear stresses developed within solders. (a)-(c) the mis-orientation maps and (d)-(f) the in-plane shear stress component within solder joints K3, M7 and C7 respectively. The experimental results were characterized at the end of 7580 cycles while the simulation results were obtained at the end of 10th cycle.

to those of K3 and C7, which arises from its larger offset distance to the neutral point (see Fig. 1) and hence harsher thermomechanical loading. The correlation between the damage developed in single crystal solder joints is quantified in Fig. 8(c) that summarizes the dependence of the SED developed upon the angle between Sn <001> and substrate normal direction (Y-axis). The difference in SED among single crystal solder joints results from the anisotropy of elasticity, coefficient of thermal expansion and plasticity, which has been shown to be affected by both its c-axis and the neutral point vector (Xu et al., 2022c).

Fig. 9 summarizes the featured stored energy density within all nine investigated multi-grain solder joints and their variants that are categorized by their microstructures. The beachball microstructure leads to significant SED peaks (see also Fig. 5 and Fig. 6). The interlaced region potentially relieves the SED peaks in the corresponding beachball microstructures (the comparison is detailed in Fig. 5, Fig. A 3 and Fig. A 4 for solder joints C7, K3 and M7, respectively). The two complex microstructures are worse, in terms of developing crack nucleation-related energy compared to a single crystal microstructure, even though a dangerous crystallographic orientation (c-axis parallel to the substrate) is assigned to the latter. Therefore, the crystal plasticity analysis suggests the optimized microstructure for solder joints subject to thermomechanical fatigue to be:

- Tailor the microstructure to be single crystal, ideally with the c-axis perpendicular to the substrate.
- If cyclic twinned microstructures are inevitable, harness the formation of interlaced regions, ideally from the top faces.
- Control the crystallographic orientations of grain(s) near the top interfaces (i.e. the package side), which has shown to be the critical region for fatigue cracking, to be c-axis perpendicular to the substrate.
- For beachball microstructure where the interlacing region is solely confined to the nucleation point or there is no interlacing, harness the beachball orientations to obtain a minimum CTE mismatch between Sn-Sn grains in the substrate plane, e.g. all cyclic Sn<001> directions lie in the substrate plane.

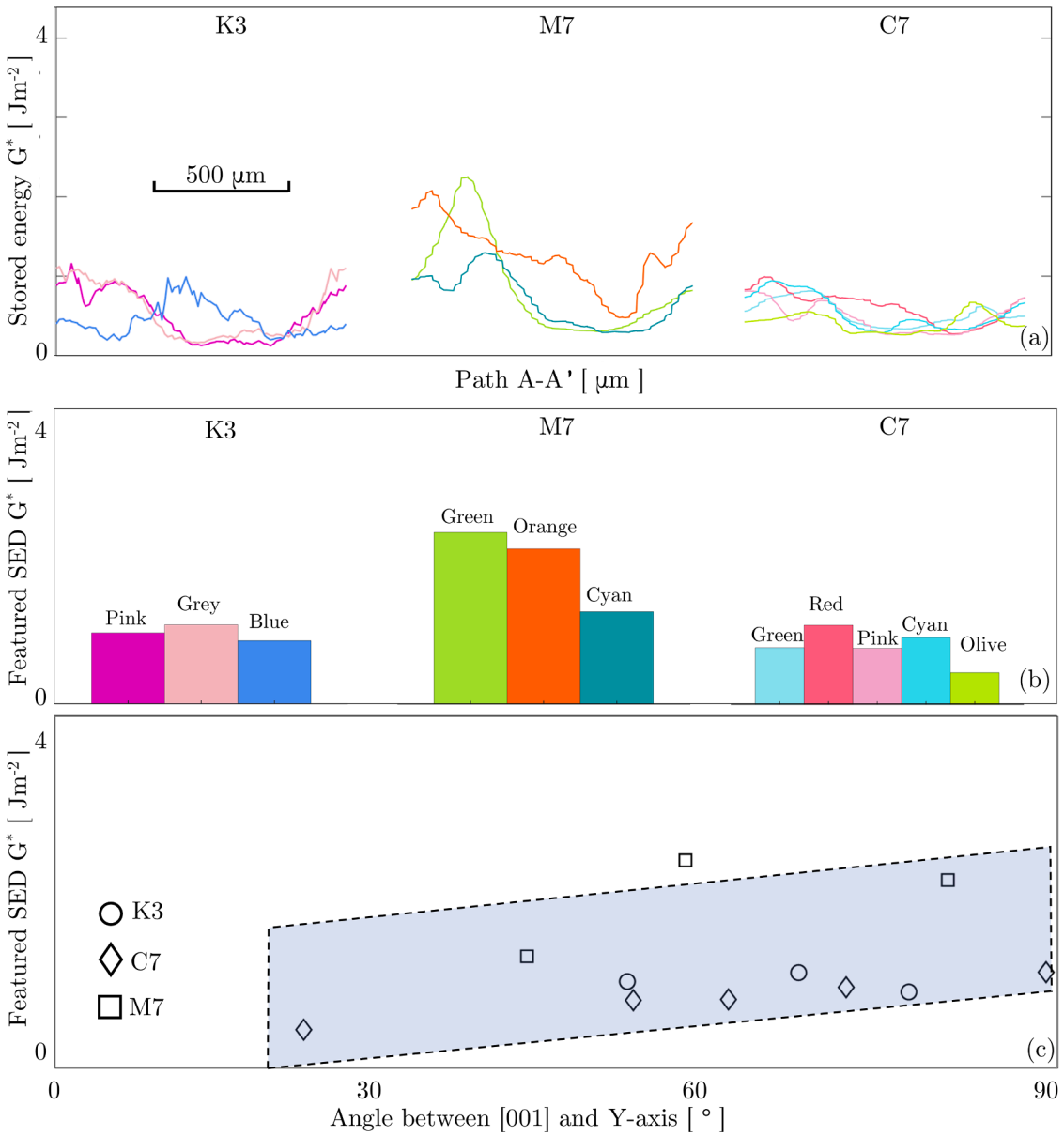


Fig. 8. The SED developed within the individual single crystal variants of solder joints K3, M7 and C7, respectively. (a) The distribution of SED along the top circumference for single crystal solders (A-A' paths refer to the same indication in Fig. 3) and (b) the featured SED that is calculated as the mean of 10% highest values ranking in (a) for the single crystal joints catagrorized by according to the EBSD characterization (shown in Fig. 2). The naming of the single crystal variants reflects their colours characterized in the IPF-X maps (see Fig. 2). (c) The correlation between the featured SED developed within the single crystal solder joints against the angle between the c-axis and the substrate.

5. Conclusions

A combined crystal plasticity finite element (CPFE) analysis with quantitative experimental characterisation has been conducted to understand the key role of microstructure in determining the micro-scale damage and failure within SAC305 ball grid array (BGA) solder joints subject to accelerated thermal cycling. Representative microstructural features, such as cyclic twinned beachball and interlaced microstructures, have been explicitly modelled and systematically studied, and their effects on the development of damage have been highlighted with comparison to the experimental evidence.

- the explicit microstructure modelling, including both the beachball grain boundaries and the interlaced regions, has captured the rank of fatigue performance of three solder joint types with representative microstructures that were quantified in the experiments.

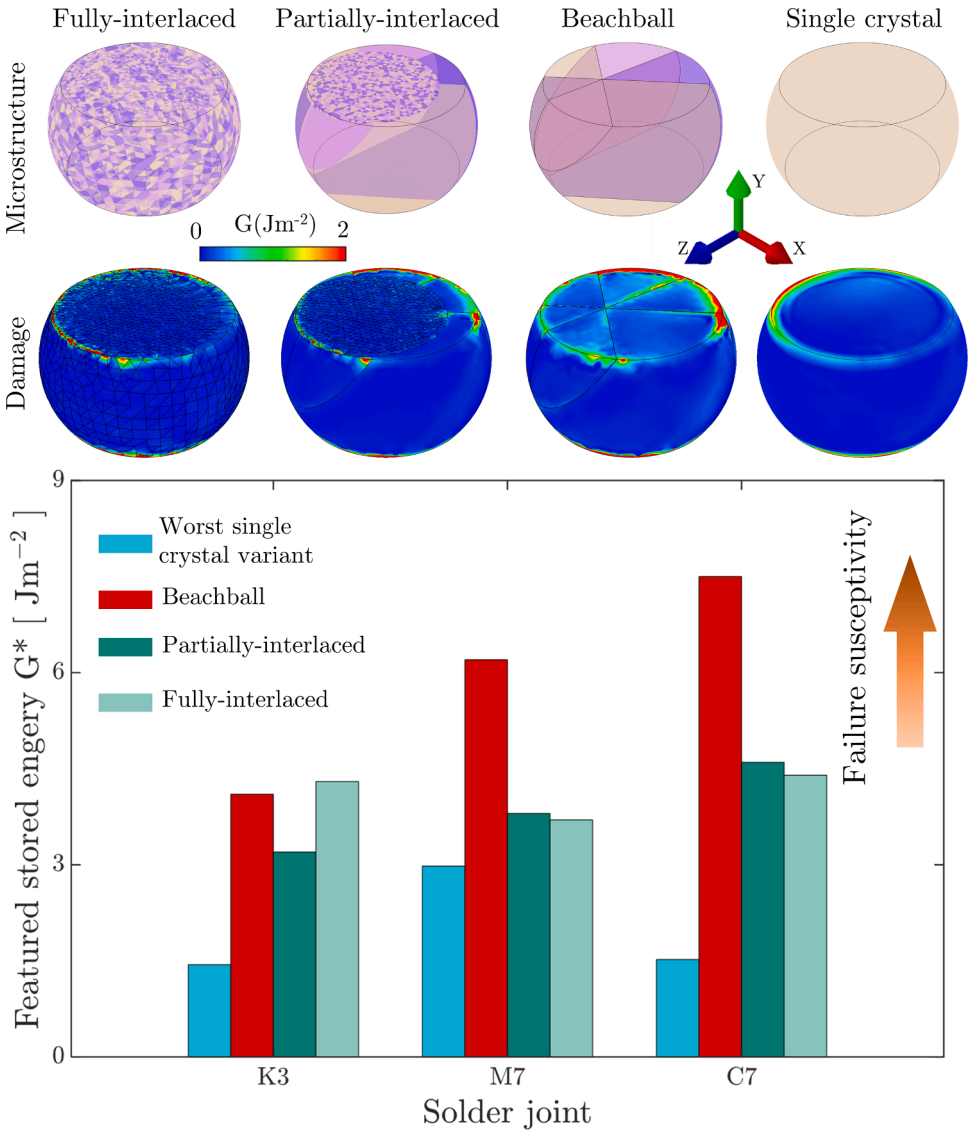


Fig. 9. The featured stored energy density (averaged for the top 10% of the full set) developed in solder joints and their variants with 10 thermal cycles. The microstructure and SED distribution of Solder Joint M7 and its variants are shown for the correlation between the microstructure and damage developed within solder joints. The worst single crystal cases (in addition to the nine multi-grain cases detailed above) are included for reference.

- The damage developed within multi-grain solder joints is found to be systematically worse compared to single crystal ones, and it is shown to arise from the localization of geometrical necessary dislocations (GND), mis-orientations (MO) and stored energy density (SED) developed near the grain boundaries.
- Interlacing, however, is found to relieve the damage localization and hence benefit the thermal fatigue life compared with beachball solder joints, which is facilitated by the microstructure inhomogeneity within the interlaced region.
- Microstructure change (mainly recrystallization) is shown to be strongly correlated to the localized shear stress concentrations, where the latter could hence be considered as a significant microstructure-sensitive mechanistic driver for solder damage and failure at the macro scale.

CRediT authorship contribution statement

Yilun Xu: Conceptualization, Formal analysis, Investigation, Methodology, Software, Writing – original draft. **Jingwei Xian:** Conceptualization, Formal analysis, Investigation, Methodology, Writing – original draft. **Richard J. Coyle:** Resources. **Christopher M. Gourlay:** Conceptualization, Funding acquisition, Writing – review & editing. **Fionn P.E. Dunne:** Conceptualization, Investigation, Methodology, Resources, Writing – review & editing.

Declaration of competing interest

The authors whose names are listed immediately below certify that they have NO affiliations with or involvement in any organization or entity with any financial interest (such as honoraria; educational grants; participation in speakers' bureaus; membership, employment, consultancies, stock ownership, or other equity interest; and expert testimony or patent-licensing arrangements), or non-financial interest (such as personal or professional relationships, affiliations, knowledge or beliefs) in the subject matter or materials discussed in this manuscript.

Data availability

Data will be made available on request.

Acknowledgement

All authors acknowledge the financial support by the Engineering and Physical Sciences Research Council for funding through the grants EP/R018863/1 and EP/R019207/1. FPED wishes to acknowledge gratefully the provision of Royal Academy of Engineering/Rolls-Royce research chair funding.

Appendix

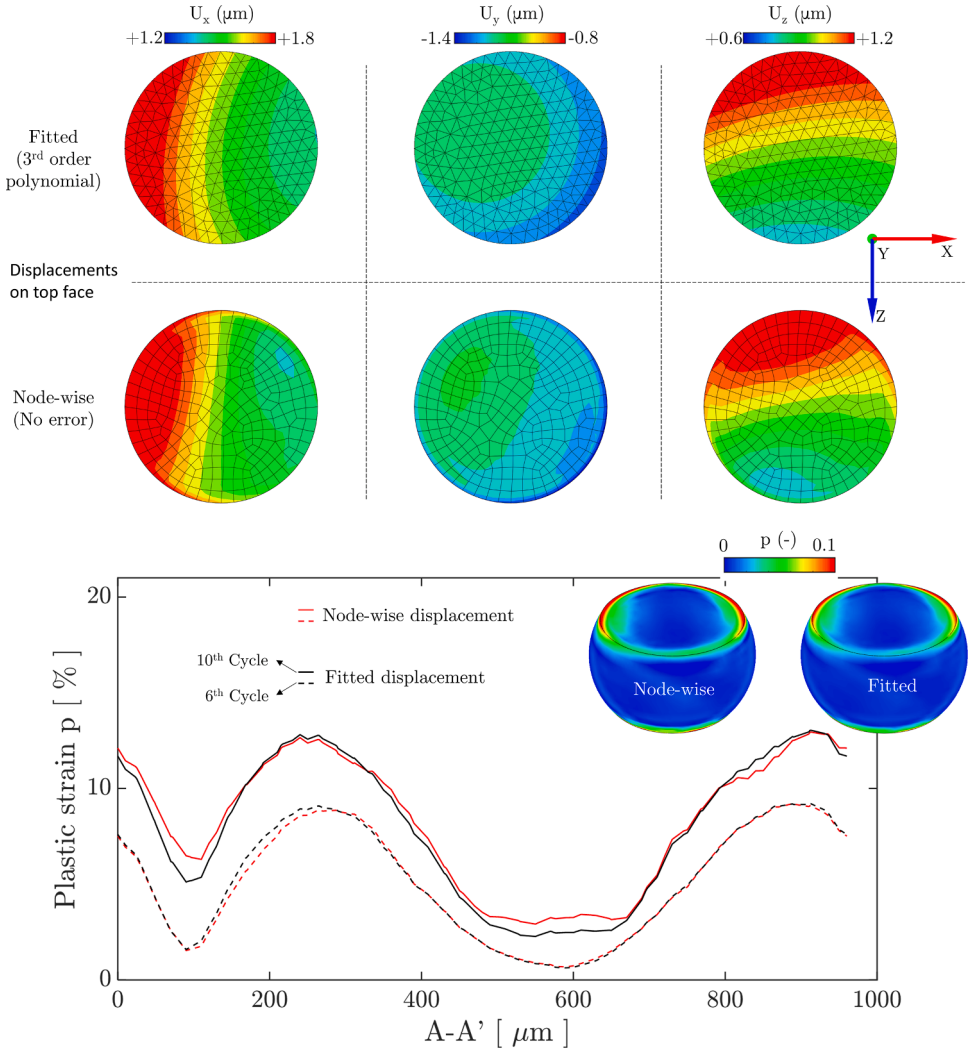


Fig. A1. The node-wise (i.e. accurate) and fitted boundary conditions (displacement fields) that were transferred from the BGA-board scale model to the individual solder joint CPFE model using a bivariate 3rd-order polynomial fitting. The error of effective plastic strains developed within solder joints (solder joint A6 taken as an example here) by imposing the fitted boundary conditions is sufficiently small.

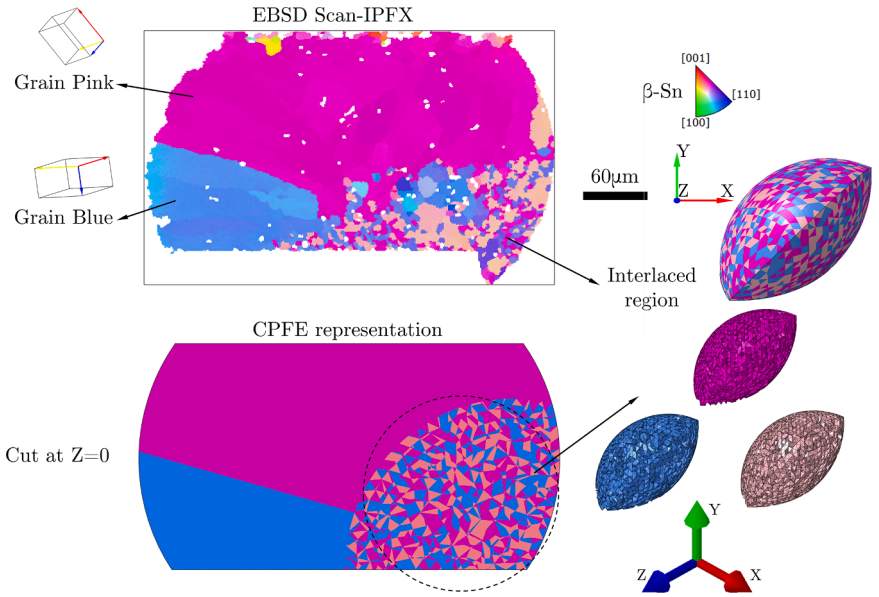


Fig. A2. The details of the interlaced region modelling of solder joint K3. The interlaced element sets are a best representation of the sizes, morphology and randomness of grains that were characterized in the experiments.

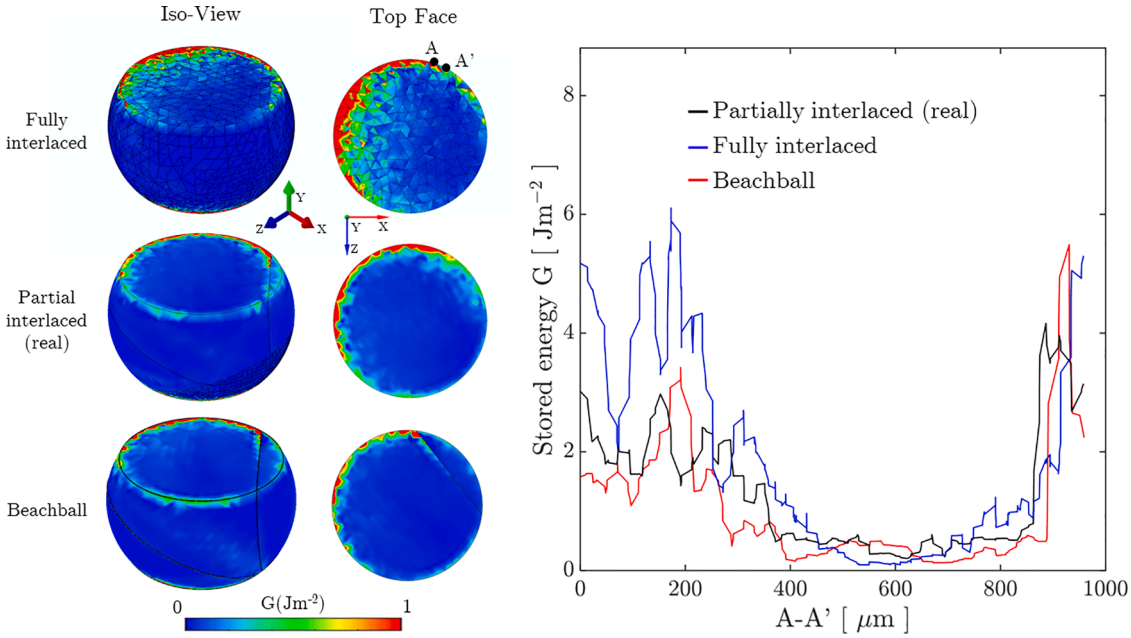


Fig. A3. The stored energy developed within solder joint K3 and its variants.

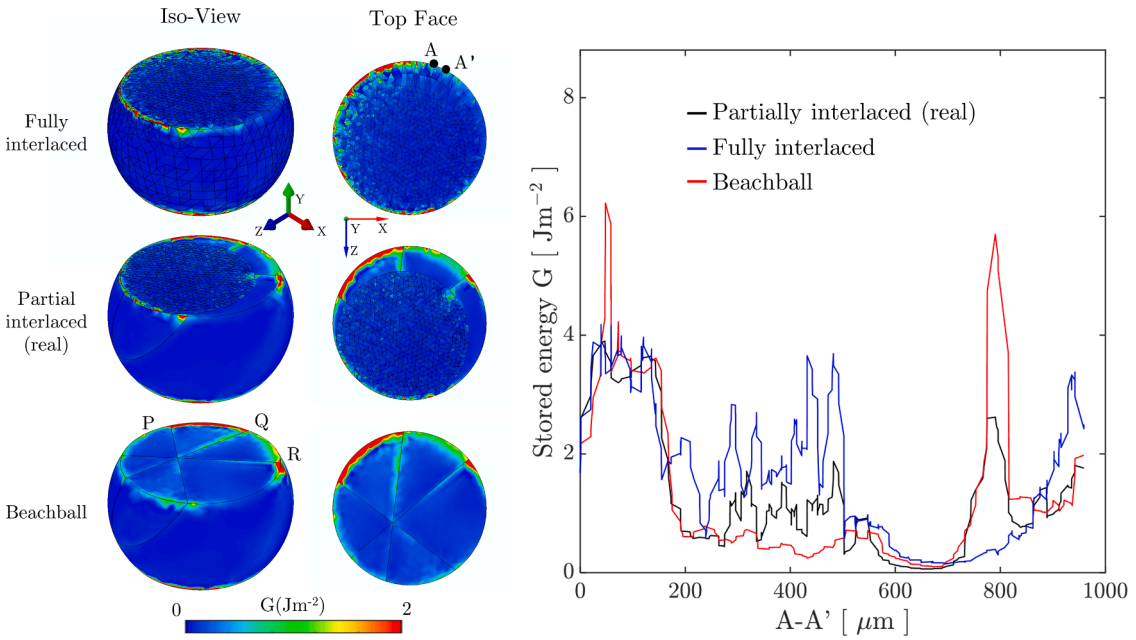


Fig. A4. The stored energy developed within solder joint M7 and its variants.

References

Arfaei, B., Anselm, M., Joshi, S., Mahin-Shirazi, S., Borgesen, P., Cotts, E., Wilcox, J., Coyle, R., 2013a. Effect of Sn grain morphology on failure mechanism and reliability of lead-free solder joints in thermal cycling tests. SMTA Int 539–550.

Arfaei, B., Mahin-Shirazi, S., Joshi, S., Anselm, M., Borgesen, P., Cotts, E., Wilcox, J., Coyle, R., 2013b. Reliability and failure mechanism of solder joints in thermal cycling tests. In: 2013 Ieee 63rd Electronic Components and Technology Conference (Ectc), pp. 976–985.

Bieler, T.R., Jiang, H.R., Lehman, L.P., Kirkpatrick, T., Cotts, E.J., Nandagopal, B., 2008. Influence of Sn grain size and orientation on the thermomechanical response and reliability of Pb-free solder joints. Ieee T. Compon. Pack T 31, 370–381. https://doi.org/10.1109/Tcapt.2008.916835.

Bieler, T.R., Zhou, B.T., Blair, L., Zamiri, A., Darbandi, P., Pourboghrat, F., Lee, T.K., Liu, K.C., 2012. The role of elastic and plastic anisotropy of Sn in recrystallization and damage evolution during thermal cycling in SAC305 solder joints. J. Electron. Mater. 41, 283–301. https://doi.org/10.1007/s11664-011-1811-x.

Borgesen, P., Wentlent, L., Hamasha, S., Khasawneh, S., Shirazi, S., Schmitz, D., Alghoul, T., Greene, C., Yin, L., 2018. A mechanistic thermal fatigue model for SnAgCu solder joints. J. Electron. Mater. 47, 2526–2544. https://doi.org/10.1007/s11664-018-6121-0.

Branch Kelly, M., Kirubanandham, A., Chawla, N., 2020. Mechanisms of thermal cycling damage in polycrystalline Sn-rich solder joints. Mater. Sci. Eng. A 771, 138614. https://doi.org/10.1016/j.msea.2019.138614.

Chen, H., Mueller, M., Mattila, T.T., Li, J., Liu, X., Wolter, K.J., Paulasto-Kröckel, M., 2011. Localized recrystallization and cracking of lead-free solder interconnections under thermal cycling. J. Mater. Res. 26, 2103–2116. https://doi.org/10.1557/jmr.2011.197.

Clech, J.-P.M., Coyle, R.J., Arfaei, B., 2019. Pb-Free solder joint thermo-mechanical modeling: state of the art and challenges. JOM 71, 143–157. https://doi.org/10.1007/s11837-018-3003-0.

Coyle, R., Parker, R., Howell, K., Hillman, D., Smetana, J., Thomas, G., Longgood, S., Osterman, M., Lundeen, E., Snugovsky10, P., 2016. A collaborative industrial consortia program for characterizing thermal fatigue reliability of third generation Pb-free alloys. SMTA Int. 25–29.

Coyle, R.J., Sweatman, K., Arfaei, B., 2015. Thermal fatigue evaluation of Pb-free solder joints: results, lessons learned, and future trends. JOM 67, 2394–2415. https://doi.org/10.1007/s11837-015-1595-1.

Darbandi, P., Bieler, T.R., Pourboghrat, F., Lee, T.K., 2013. Crystal plasticity finite-element analysis of deformation behavior in multiple-grained lead-free solder joints. J. Electron. Mater. 42, 201–214. https://doi.org/10.1007/s11664-012-2339-4.

Darbandi, P., Lee, T.K., Bieler, T.R., Pourboghrat, F., 2014. Crystal plasticity finite element study of deformation behavior in commonly observed microstructures in lead free solder joints. Comp. Mater. Sci. 85, 236–243. https://doi.org/10.1016/j.commatsci.2014.01.002.

Dunne, F.P.E., Rugg, D., Walker, A., 2007. Lengthscale-dependent, elastically anisotropic, physically-based hcp crystal plasticity: application to cold-dwell fatigue in Ti alloys. Int. J. Plast. 23, 1061–1083. https://doi.org/10.1016/j.ijplas.2006.10.013.

Gu, T., Xu, Y., Gourlay, C.M., Britton, T.B., 2020. In-situ electron backscatter diffraction of thermal cycling in a single grain Cu/Sn-3Ag-0.5Cu/Cu solder joint. Scripta Mater 175, 55–60. https://doi.org/10.1016/j.scriptamat.2019.09.003.

Haug, C., Molodov, D., Gumbsch, P., Greiner, C., 2022. Tribologically induced crystal rotation kinematics revealed by electron backscatter diffraction. Acta Mater. 225 https://doi.org/10.1016/j.actamat.2021.117566.

Jiang, J., Yang, J., Zhang, T., Zou, J., Wang, Y., Dunne, F.P.E., Britton, T.B., 2016. Microstructurally sensitive crack nucleation around inclusions in powder metallurgy nickel-based superalloys. Acta Mater. 117, 333–344. https://doi.org/10.1016/j.actamat.2016.07.023.

Jiang, Q., Deshpande, A., Dasgupta, A., 2022. Multi-scale crystal viscoplasticity approach for estimating anisotropic steady-state creep properties of single-crystal SnAgCu alloys. Int. J. Plast. 153, 103271 https://doi.org/10.1016/j.ijplas.2022.103271.

Kamlah, M., Haupt, P., 1997. On the macroscopic description of stored energy and self heating during plastic deformation. Int. J. Plast. 13, 893–911. https://doi.org/10.1016/S0749-6419(97)00063-6.

Kysar, J.W., Gan, Y.X., Morse, T.L., Chen, X., Jones, M.E., 2007. High strain gradient plasticity associated with wedge indentation into face-centered cubic single crystals: geometrically necessary dislocation densities. J. Mech. Phys. Solids 55, 1554–1573. https://doi.org/10.1016/j.jmps.2006.09.009.

Lehman, L.P., Xing, Y., Bieler, T.R., Cotts, E.J., 2010. Cyclic twin nucleation in tin-based solder alloys. Acta Mater. 58, 3546–3556. https://doi.org/10.1016/j.actamat.2010.01.030.

Li, X.Y., Lu, L., Li, J.G., Zhang, X., Gao, H.J., 2020. Mechanical properties and deformation mechanisms of gradient nanostructured metals and alloys. Nat. Rev. Mater. 5, 706–723. https://doi.org/10.1038/s41578-020-0212-2.
Lövberg, A., Tegehall, P.E., Wetter, G., Brinkfeldt, K., Andersson, D., 2017. Simulations of the impact of single-grained lead-free solder joints on the reliability of ball Grid Array components. In: 2017 18th International Conference on Thermal, Mechanical and Multi-Physics Simulation and Experiments in Microelectronics and Microsystems (EuroSimE), pp. 1–10.
Ma, Z.L., Belyakov, S.A., Sweatman, K., Nishimura, T., Nishimura, T., Gourlay, C.M., 2017. Harnessing heterogeneous nucleation to control tin orientations in electronic interconnections. Nat. Commun. 8, 1916. https://doi.org/10.1038/s41467-017-01727-6.
Matin, M.A., Coenen, E.W.C., Vellinga, W.P., Geers, M.G.D., 2005. Correlation between thermal fatigue and thermal anisotropy in a Pb-free solder alloy. Scripta Mater 53, 927–932. https://doi.org/10.1016/j.scriptamat.2005.06.034.
Pantleon, W., 2008. Resolving the geometrically necessary dislocation content by conventional electron backscattering diffraction. Scripta Mater 58, 994–997. https://doi.org/10.1016/j.scriptamat.2008.01.050.
Prastiti, N.G., Xu, Y., Balint, D.S., Dunne, F.P.E., 2020. Discrete dislocation, crystal plasticity and experimental studies of fatigue crack nucleation in single-crystal nickel. Int. J. Plast. 126, 102615 https://doi.org/10.1016/j.ijplas.2019.10.003.
Qi, L.H., Huang, H.H., Zhao, X.K., Zhang, H., 2009. Effect of thermal-shearing cycling on Ag3Sn microstructural coarsening in SnAgCu solder. J. Alloy. Compound. 469, 102–107. https://doi.org/10.1016/j.jallcom.2008.01.108.
Ruebeling, F., Xu, Y., Richter, G., Dini, D., Gumbsch, P., Greiner, C., 2021. Normal load and counter body size influence the initiation of microstructural discontinuities in copper during sliding. ACS Appl. Mater. Interfaces 13, 4750–4760. https://doi.org/10.1021/acsami.0c19736.
Shang, H., Ma, Z.L., Belyakov, S.A., Gourlay, C.M., 2017. Grain refinement of electronic solders: the potential of combining solute with nucleant particles. J. Alloy. Compound. 715, 471–485. https://doi.org/10.1016/j.jallcom.2017.04.268.
Sidhu, R.S., Chawla, N., 2008. Thermal fatigue behavior of Sn-rich (Pb-Free) solders. Metall. Mater. Trans. A 39a 799-810. https://doi.org/10.1007/s11661-008-9480-y.
Stoyanov, S., Bailey, C., Stewart, P., Morrison, G., 2020. Reliability impact of assembly materials for Micro-BGA components in high reliability applications. In: 2020 IEEE 8th Electronics System-Integration Technology Conference (ESTC). IEEE, pp. 1–7.
Sundelin, J.J., Nurmi, S.T., Lepisto, T.K., 2008. Recrystallization behaviour of SnAgCu solder joints. Mat. Sci. Eng. A-Struct. 474, 201–207. https://doi.org/10.1016/j.msea.2007.04.013.
Wan, V.V.C., MacLachlan, D.W., Dunne, F.P.E., 2014. A stored energy criterion for fatigue crack nucleation in polycrystals. Int. J. Fatigue 68, 90–102. https://doi.org/10.1016/j.ijfatigue.2014.06.001.
Wan, W., Xu, Y., Yu, X., Dunne, F.P.E., 2023. Microstructurally-sensitive fatigue crack nucleation in a Zircaloy-4 alloy. J. Mech. Phys. Solids 180, 105417. https://doi.org/10.1016/j.jmps.2023.105417.
Wilson, D., Dunne, F.P.E., 2019. A mechanistic modelling methodology for microstructure-sensitive fatigue crack growth. J. Mech. Phys. Solids 124, 827–848. https://doi.org/10.1016/j.jmps.2018.11.023.
Witzen, W.A., Polonsky, A.T., Pollock, T.M., Beyerlein, I.J., 2020. Three-dimensional maps of geometrically necessary dislocation densities in additively manufactured Ni-based superalloy IN718. Int. J. Plast. 131 https://doi.org/10.1016/j.ijplas.2020.102709.
Xia, W.Z., Patil, P.P., Liu, C., Dehm, G., Brinckmann, S., 2023. A novel microwall sliding test uncovering the origin of grain refined tribolayers. Acta Mater. 246, 118670 https://doi.org/10.1016/j.actamat.2023.118670.
Xian, J.W., Ma, Z.L., Belyakov, S.A., Ollivier, M., Gourlay, C.M., 2017. Nucleation of tin on the Cu6Sn5 layer in electronic interconnections. Acta Mater. 123, 404–415. https://doi.org/10.1016/j.actamat.2016.10.008.
Xian, J.W., Xu, Y., Stoyanov, S., Coyle, R.J., Dunne, F.P.E., Gourlay, C.M., 2023. arXiv preprint. https://doi.org/10.48550/arXiv.2311.03891.
Xie, M.W., Chen, G., 2022. A developed crystal plasticity model for viscoplastic mechanical behavior of SAC305 solder under thermomechanical coupled cyclic loading. Int. J. Plast. 159, 103465 https://doi.org/10.1016/j.ijplas.2022.103465.
Xie, M.W., Chen, G., Yang, J., Xu, W.L., 2021. Temperature- and rate-dependent deformation behaviors of SAC305 solder using crystal plasticity model. Mech. Mater. 157 https://doi.org/10.1016/j.mechmat.2021.103834.
Xie, M.W., Chen, G., Yu, J.T., Wu, Y.T., Liu, X., Yang, J., Xu, W.L., 2022. A dual-phase crystal plasticity finite-element method for modeling the uniaxial deformation behaviors of thermally aged SAC305 solder. Int. J. Plast. 155, 103342 https://doi.org/10.1016/j.ijplas.2022.103342.
Xu, Y., 2021. A non-local methodology for geometrically necessary dislocations and application to crack tips. Int. J. Plast. 140, 102970 https://doi.org/10.1016/j.ijplas.2021.102970.
Xu, Y., Balint, D.S., Greiner, C., Dini, D., 2022a. On the origin of plasticity-induced microstructure change under sliding contacts. Friction 11, 473–488. https://doi.org/10.1007/s40544-022-0624-7.
Xu, Y., Gu, T., Xian, J., Giuliani, F., Ben Britton, T., Gourlay, C.M., Dunne, F.P.E., 2021a. Intermetallic size and morphology effects on creep rate of Sn-3Ag-0.5Cu solder. Int. J. Plast. 137, 102904 https://doi.org/10.1016/j.ijplas.2020.102904.
Xu, Y., Gu, T., Xian, J., Giuliani, F., Ben Britton, T., Gourlay, C.M., Dunne, F.P.E., 2022b. Multi-scale plasticity homogenization of Sn–3Ag-0.5Cu: from β-Sn micropillars to polycrystals with intermetallics. Mater. Sci. Eng. A 855, 143876. https://doi.org/10.1016/j.msea.2022.143876.
Xu, Y., Lu, X., Yang, X., Li, W., Aitken, Z., Vastola, G., Gao, H., Zhang, Y.W., 2024. Temperature-dependent, multi-mechanism crystal plasticity reveals the deformation and failure behaviour of multi-principal element alloys. J. Mech. Phys. Solids 185, 105549. https://doi.org/10.1016/j.jmps.2024.105549.
Xu, Y., Ruebeling, F., Balint, D., Greiner, C., Dini, D., 2021b. On the origin of microstructural discontinuities in sliding contacts: a discrete dislocation plasticity analysis. Int. J. Plast. 138 https://doi.org/10.1016/j.ijplas.2021.102942.
Xu, Y., Wan, W., Dunne, F.P.E., 2021c. Microstructural fracture mechanics: stored energy density at fatigue cracks. J. Mech. Phys. Solids 146, 104209. https://doi.org/10.1016/j.jmps.2020.104209.
Xu, Y.L., Xian, J.W., Stoyanov, S., Bailey, C., Coyle, R.J., Gourlay, C.M., Dunne, F.P.E., 2022c. A multi-scale approach to microstructure-sensitive thermal fatigue in solder joints. Int. J. Plast. 155, 103308 https://doi.org/10.1016/j.ijplas.2022.103308.
Yao, Y., Long, X., Keer, L.M., 2017. A review of recent research on the mechanical behavior of lead-free solders. Appl. Mech. Rev. 69 https://doi.org/10.1115/1.4037462.
Zhang, X.X., Stinville, J.C., Pollock, T.M., Dunne, F.P.E., 2021. Crystallography and elastic anisotropy in fatigue crack nucleation at nickel alloy twin boundaries. J. Mech. Phys. Solids 155. https://doi.org/10.1016/j.jmps.2021.104538.
Zhang, Y.H., Gao, Y.F., Nicola, L., 2014. Lattice rotation caused by wedge indentation of a single crystal: dislocation dynamics compared to crystal plasticity simulations. J. Mech. Phys. Solids 68, 267–279. https://doi.org/10.1016/j.jmps.2014.04.006.
Zhou, B., Bieler, T.R., Lee, T.K., Liu, K.C., 2009. Methodology for analyzing slip behavior in ball grid array lead-free solder joints after simple shear. J. Electron. Mater. 38, 2702–2711. https://doi.org/10.1007/s11664-009-0929-6.
Zhou, B.T., Zhou, Q., Bieler, T.R., Lee, T.K., 2015. Slip, crystal orientation, and damage evolution during thermal cycling in high-strain wafer-level chip-scale packages. J. Electron. Mater. 44, 895–908. https://doi.org/10.1007/s11664-014-3572-9.
Zhu, Y., Wu, X., 2023. Heterostructured materials. Prog. Mater Sci. 131, 101019 https://doi.org/10.1016/j.pmatsci.2022.101019.